PHOTOSYNTHETICA
International Journal for Photosynthesis Research

DOI 10.32615/ps.2025.030 PHOTOSYNTHETICA 64 (1): 1-11, 2026

Characterizing the CO_2-response curve in photosynthesis and photorespiration: an innovative model for C_3 plant species

H.-J. KANG[*,**,†], T. AN[***,#,†], X.-L. YANG[##,###], Z.-P. YE[***,§,+], and F.-B. WANG[§,+]

Wenzhou Academy of Agricultural Sciences, Wenzhou, Zhejiang, China[*]
Wenzhou Key Laboratory of Agricultural & Forestry Carbon Sequestration and Tea Resource Development, Wenzhou, Zhejiang, China[**]
New Quality Productivity Research Center, Guangdong ATV College of Performing Arts, Deqing, Guangdong, China[***]
Medical College, Guangdong ATV College of Performing Arts, Deqing, Guangdong, China[#]
School of Life Sciences, Nantong University, Nantong, Jiangsu, China[##]
State Key Laboratory of Environmental Chemistry and Ecotoxicology, Research Center for Eco-Environmental Sciences, Chinese Academy of Sciences, Beijing, China[###]
Institute of Biophysics, Math & Physics College, Jinggangshan University, Ji'an, Jiangxi, China[§]

Abstract

We introduce a novel model for characterizing the CO_2-response curve in photosynthesis, addressing the limitations of the Farquhar–von Caemmerer–Berry (FvCB) model by providing a more comprehensive framework for understanding photosynthetic responses to varying CO_2 concentrations in C_3 plants. The FvCB model, while instrumental in interpreting the photosynthetic response to CO_2, does not directly estimate critical parameters such as maximum net photosynthetic rate, transit point from RuBP- to TPU-limited photosynthesis, and the CO_2 compensation point in the presence of day respiration (R_{day}). Our new model, referred to as Model I, incorporates these parameters and accounts for the R_{day}, offering a nuanced understanding of plant physiological responses to CO_2 concentrations. The research also developed Model II, which does not require an explicit R_{day}, addressing the challenges in measuring R_{day} and providing an alternative for analyzing the CO_2-response curve. Both models were validated against empirical data, demonstrating their effectiveness in studying plant photosynthesis and photorespiration. The study concludes that the new models advance the FvCB model by predicting photosynthetic and photorespiratory responses under varying conditions, which is crucial for agricultural practices and ecosystem management in the context of climate change.

Keywords: C_3 plants; C_4 plants; climate change; CO_2-response curve; Farquhar–von Caemmerer–Berry model; photosynthesis.

Highlights

- Model I improves FvCB by estimating P_{Nmax}, $C_{a,TPU}$, and Γ with R_{day} integration
- Model II offers a R_{day}-free alternative for CO_2-response analysis, easing measurement challenges
- Both models improve photosynthetic understanding, aiding climate-resilient agriculture

Received 5 July 2025
Accepted 25 September 2025
Published online 30 October 2025

[+]Corresponding authors
e-mail: yezp@jgsu.edu.cn
wfb19872856@163.com

Abbreviations: C_a – atmospheric CO_2 concentration; $C_{a,TPU}$ – C_a transit points from RuBP- to TPU-limited photosynthesis; C_i – intercellular CO_2 concentration; $C_{i,TPU}$ – C_i transit points from RuBP- to TPU-limited photosynthesis; FvCB – Farquhar–von Caemmerer–Berry (FvCB) model; g_m – mesophyll conductance; I – light intensity; I_{sat} – saturation light intensity corresponding to P_N; J – electron transport rate; J_{max} – maximum electron transport rate estimated by FvCB model; P_N – net photosynthetic rate; P_N–C_a – ambient CO_2-response curve of photosynthesis; P_N–C_i – intercellular CO_2-response curve of photosynthesis; P_N–I – light-response curve of photosynthesis; P_{Nmax} – maximum net photosynthetic rate; R_{day} – day respiratory rate; R_p – photorespiratory rate; R_p–C_a – ambient CO_2-response curve of R_p; R_{pa} – apparent photorespiratory rate; R_{pa}–C_i – intercellular CO_2-response curve of R_{pa}; R_{p0} – photorespiratory rate at C_a or C_i = 0 μmol mol^{-1}; R_{pa0} – apparent photorespiratory rate at C_a or C_i = 0 μmol mol^{-1}; V_c – rate of carboxylation; V_{cmax} – maximum velocities of the carboxylase; V_o – rate of oxygenation; V_{TPU} – triose phosphate utilization rate; α_c – initial slope of CO_2-response curve of photosynthesis; β_c – photoinhibition coefficient; γ_c – saturated coefficient; Γ – photorespiratory CO_2-compensation point in the presence of R_{day}; Γ_* – photorespiratory CO_2-compensation point in the absence of R_{day}.

Acknowledgements: This research was supported by the Natural Science Foundation of China (Grant No. 32260063 and 32060428), the Natural Science Foundation of Jiangxi Province (Grant No. 20224BAB205020).

[†]These authors have contributed equally to this work.

Conflict of interest: The authors declare that they have no conflict of interest.

Introduction

In the field of plant physiological ecology, CO_2-response models are foundational, offering a holistic framework for interpreting and forecasting plant reactions to atmospheric CO_2 fluctuations (Vialet-Chabrand *et al.* 2017, Kromdijk *et al.* 2019, Ye *et al.* 2025b). These models are indispensable for grasping the complex interplay between environmental factors and the photosynthetic machinery within plants, varying in complexity from straightforward to intricate. They have been instrumental in predicting photosynthesis and demystifying processes that were once enigmatic (Farazdaghi and Edwards 1988, Sharkey *et al.* 2007, Gregory *et al.* 2021).

Currently, photosynthetic CO_2-response models are divided into two main categories. The first category includes classical models, such as the rectangular hyperbola model and the Michaelis–Menten model (Wu *et al.* 2020, Kieffer *et al.* 2024, Hu *et al.* 2025). The second category comprises mechanistic models, with key representatives being the C_3 biochemical model developed by Farquhar *et al*. (1980), known as the FvCB model, and the C_4 biochemical model crafted by Peisker (1986), referred to as the C_4 model. It is important to note that the model presented by Farquhar *et al.* (1980) provided the core biochemical framework. This framework has since been expanded and refined by the scientific community to include other key limitations, most notably the triose phosphate utilization (TPU) limitation (Harley and Sharkey 1991, Gregory *et al.* 2021) and the explicit consideration of mesophyll conductance (g_m) (Long and Bernacchi 2003, Barbour *et al.* 2016, Flexas *et al.* 2016). Throughout this manuscript, we refer to this evolved and comprehensive framework as the 'FvCB model'.

Classical models, which disregard the biochemical processes of plant photosynthesis, deduce parameters such as the maximum net photosynthetic rate (P_{Nmax}), CO_2-compensation point (Γ) in the presence of day respiratory rate (R_{day}), and the apparent photorespiration rate (R_{pa0}) including R_{day} under the assumption that ambient CO_2 is set to 0 μmol mol^{-1} by fitting the photosynthetic CO_2-response curve (P_N–C_i or P_N–C_a curve; C_i is the intercellular CO_2 concentration, C_a is the ambient CO_2 concentration). Researchers utilize these parameters to depict the photosynthetic characteristics of plants under diverse environmental conditions (Li *et al.* 2019, Joubert *et al.* 2023, Ye *et al.* 2024b). However, previous studies have indicated that both the rectangular hyperbola model and the Michaelis–Menten model significantly overestimated P_{Nmax} (Zheng *et al*. 2012, Sun *et al*. 2015, Poirier-Pocovi *et al*. 2018). Moreover, the investigation into the response pattern of the apparent photorespiration rate (R_{pa}), encompassing the R_{day}, to fluctuating ambient CO_2 concentrations, remains a significantly underexplored area. Undertaking quantitative research to elucidate how R_{pa} in plants reacts to CO_2 is of profound significance and immense value. Such research offers vital insights into the impacts of escalating global atmospheric CO_2 concentrations on the processes of carbon assimilation metabolism.

In contrast, the FvCB model, through analysis of the P_N–C_i curve under saturation irradiance, yields parameters such as the maximum carboxylation efficiency (V_{cmax}), the maximum rate of electron transport (J_{max}), triose phosphate utilization (V_{TPU}), the CO_2-compensation point (Γ_*) in the absence of R_{day}, and mesophyll conductance (g_m). These parameters are vital for a comprehensive analytical framework that quantitatively differentiates between biochemical and stomatal limitations on the CO_2 response of photosynthesis (Long and Bernacchi 2003, Dubois *et al*. 2007, Yin *et al*. 2004, 2009, 2021; Yin and Amthor 2024, Ye *et al.* 2025b). By integrating these parameters, researchers can gain a deeper understanding of the dynamic behavior of photosynthesis and its regulation under various conditions, essential for predicting plant growth and productivity amidst global climate change and for developing strategies to enhance carbon sequestration and food security (Joshi *et al*. 2022, Xue *et al*. 2022, Chang *et al*. 2023, Liu *et al*. 2024).

However, the FvCB model has some limitations. Specifically, it is unable to directly estimate several key photosynthetic parameters, such as P_{Nmax}, the transition point from RuBP- to TPU-limited photosynthesis ($C_{i,TPU}$), Γ, and R_{pa0}. Moreover, the model fails to characterize the CO_2 response of R_{pa} (*i.e.*, R_{pa}–C_i or R_{pa}–C_a curve). Parameters, such as P_{Nmax}, $C_{i,TPU}$, R_{pa0}, and Γ, are typically measured using advanced photosynthetic measurement instruments, which provide detailed insights into the photosynthetic process under diverse environmental conditions (Rizza *et al*. 2001, Lawson *et al*. 2002). This limitation has spurred significant efforts to develop new models that can more accurately represent C_3 photosynthesis, accounting for the dynamic nature of photosynthetic responses to environmental changes (Baker 2008). Advances in measurement techniques, as described in various studies, have enabled more precise determination of these parameters, which are crucial for a comprehensive understanding of plant physiological processes and their ecological implications (Baker 2008).

The objective of this research is to develop and validate a novel, comprehensive CO_2-response model for plant photosynthesis that accurately reflects the complex physiological processes, dynamic behavior of photosynthesis, and photorespiration under varying environmental conditions. This model aims to overcome the limitations of the FvCB model, particularly its inability to directly estimate certain critical photosynthetic parameters, such as P_{Nmax}, $C_{i,TPU}$, Γ, and R_{pa0}. Additionally, our model seeks to address the FvCB model's shortcomings in accurately depicting R_{pa}–C_i or R_{pa}–C_a curve, offering a more nuanced understanding of plant physiological responses in diverse environmental contexts.

In pursuit of these goals, we have established two critical objectives: (*1*) model reproduction accuracy: the primary goal is to ascertain whether the new model can accurately replicate the actual measured CO_2-response curves of photosynthesis (P_N–C_i) for a diverse array of plant species, including four C_3 species – *Ipomoea batatas* (L.) Lam., *Pachyrhizus erosus* (L.) Urb.,

Capsicum annuum L., and *Abelmoschus esculentus* (L.); (*2*) consistency of photosynthetic parameters: we aim to evaluate the consistency of key photosynthetic parameters – such as P_{Nmax}, $C_{i,TPU}$, Γ, and R_{pa0} – derived from fitting the P_N–C_i or P_N–C_a curves with the new model, against observed values. We assessed whether these parameters align closely with empirical data, indicating no significant discrepancies between model-fitted values and observed values. Compliance with these conditions will establish the model as a dependable tool for analyzing photosynthetic traits of plants under various environmental conditions. The development of such comprehensive models is crucial for enhancing our insights into plant responses to atmospheric CO_2 fluctuations and for improving predictions of primary productivity and carbon cycling within ecosystems. Ultimately, this integrated approach will provide invaluable insights into the adaptive strategies and resilience of plants in response to climate change.

Materials and methods

Study site and plants: The experiment was conducted at the experimental base of the Agricultural Science Research Institute in Wenzhou, Zhejiang Province. In this study, *I. batatas*, *P. erosus*, *C. annuum*, and *A. esculentus* were used as experimental materials. Except *P. erosus*, which was propagated through cuttings, all other materials were grown from seedlings. *I. batatas*, *C. annuum*, and *A. esculentus* were sown by the end of February 2024 and subsequently transplanted in mid-March 2024. *P. erosus* cuttings were prepared on 25 April 2024. All materials were planted outdoors in standard garden soil with a pH of approximately 6.8 and an available nitrogen content of around 150 mg kg^{-1}. The plants were managed using conventional agricultural practices.

Data collection spanned from 7 July to 23 July 2024. During this period, *C. annuum* plants had reached a height of approximately 45 cm, while *A. esculentus* plants reached *ca.* 70 cm. *I. batatas* were growing in a prostrate manner, whereas *P. erosus* was cultivated with the support of trellises. All plants were in a robust stage of vegetative growth. The leaves selected for measurement were fully expanded and well-formed. For *I. batatas*, the 8th to 10th mature leaves from the top on the main stem were chosen; for *P. erosus*, the 5th compound leaf counting from the bottom upwards; for *C. annuum*, the 4th fully expanded leaf counting from the top downwards; and for *A. esculentus*, the 3rd fully expanded leaf counting from the top downwards. A total of seven plants of each species were selected for the testing process.

Model description

A new model for describing the CO_2-response curve of photosynthesis with an explicit R_{day}: Farquhar *et al.* (1980) showed that the rate of net carbon assimilation in C_3 leaves, or P_N, depends on light, CO_2, temperature, and humidity, as well as internal leaf processes. The P_N can be limited by: (*1*) Rubisco-catalyzed carboxylation, the first step in converting CO_2 into sugars. (*2*) The regeneration of RuBP, influenced by the electron transport rate. (*3*) The utilization of triose phosphates, or TPU, which, if slow, can inhibit carboxylation.

In the FvCB model (Farquhar *et al.* 1980), P_N is given as:

$$P_N = V_c - 0.5V_o - R_{day} \quad (1)$$

where P_N is the net photosynthetic rate (unit: μmol m^{-2} s^{-1}), V_c is the rate of carboxylation, and V_o is the rate of oxygenation (unit: μmol m^{-2} s^{-1}) (Farquhar *et al.* 1980, Farquhar and Busch 2017). The multiplier of 0.5 in Eq. 1 indicates that 0.5 mol of CO_2 is released in the photorespiratory pathway for every mol of RuBP oxygenated. R_{day} is the day respiratory rate (unit: μmol m^{-2} s^{-1}).

According to the FvCB model (Farquhar *et al.* 1980), Eq. 1 can be expressed as:

$$P_N = V_c - 0.5V_o - R_{day} = V_c\left(1 - \frac{\Gamma_*}{C_i}\right) - R_{day} \quad (2)$$

where C_i is the intercellular CO_2 concentration (unit: μmol mol^{-1}); Γ_* (unit: μmol mol^{-1}) is the CO_2-compensation point in the absence of R_{day} (Farquhar *et al.* 1980, Long and Bernacchi 2003).

Leveraging the established FvCB model as our framework, we have diligently developed a new model that describes precisely the CO_2 response in photosynthesis. The formulation of this advanced CO_2-response model for photosynthesis, which we will refer to as Model I, is expressed as follows:

$$P_N = \alpha_c \frac{1 - \beta_c C_i}{1 + \gamma_c C_i}(C_i - \Gamma_*) - R_{day} \quad (3)$$

where α_c (unit: mol m^{-2} s^{-1}), β_c (unit: μmol^{-1} mol), and γ_c (unit: μmol^{-1} mol) are three coefficients that depend on plant characteristics and environmental conditions, and they are independent of C_i. Furthermore, the term C_i in Eqs. 2 and 3 can be substituted with the ambient CO_2 concentration, denoted as C_a.

Fig. 1 shows the influence of coefficient values (β_c and γ_c for Model I) on model simulations when α_c = 0.05 mol m^{-2} s^{-1}, Γ_* = 20 μmol mol^{-1}, and R_{day} = 3.5 μmol m^{-2} s^{-1}. Fig. 1 illustrates that when the value of γ_c is kept constant, an increase in the value of β_c results in a more pronounced curvature of the resulting curve and a steeper rate of decline in net photosynthesis as C_i increases (Fig. 1*A*). Conversely, when the value of β_c remains unchanged, an increased value of γ_c results in a less curved profile of the resulting graph and a more gradual rate of increase in net photosynthesis with rising C_i concentrations (Fig. 1*B*). Hence, β_c is referred to as the oxygenation term, while γ_c is recognized as the saturation term, within this context. Furthermore, Fig. 1 demonstrates that P_N varies smoothly in response to changes in the C_i variable.

In addition, according to Eq. 1 or Eq. 2, Eq. 3 can be rearranged as:

$$P_N = \alpha_c \frac{1 - \beta_c C_i}{1 + \gamma_c C_i} C_i - \alpha_c \frac{1 - \beta_c C_i}{1 + \gamma_c C_i} \Gamma - R_{day} \quad (4)$$

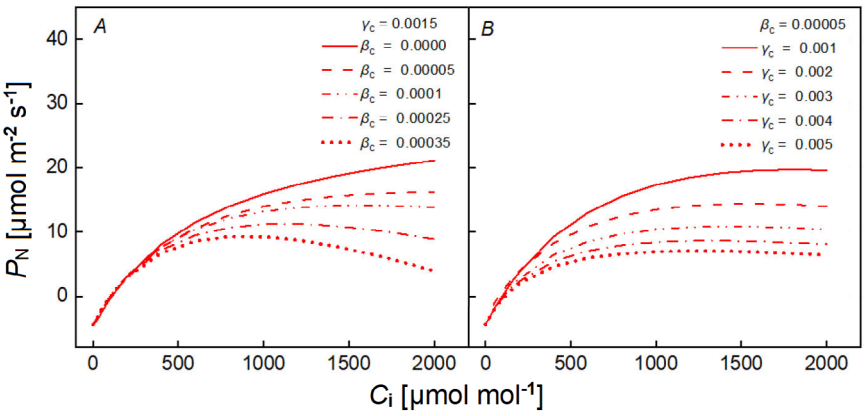

Fig. 1. Influence of coefficient values (β_c and γ_c for Model I) on model simulations when α_c = 0.05 mol m^{-2} s^{-1}, Γ_* = 20 μmol mol^{-1}, and R_{day} = 3.5 μmol m^{-2} s^{-1}. The variations of coefficient values are presented as follows: (*A*) β_c and (*B*) γ_c.

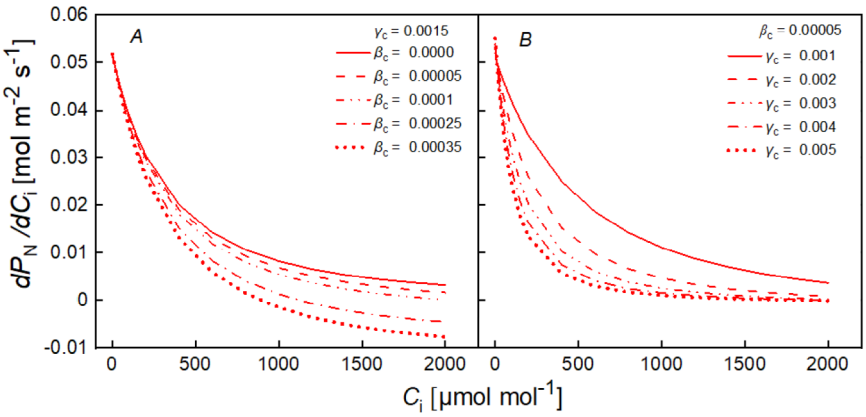

Fig. 2. Variation of dP_N/dC_i with C_i for different coefficient values (β_c and γ_c) in Model I at α_c = 0.05 mol m^{-2} s^{-1}, Γ_* = 20 μmol mol^{-1}, and R_{day} = 3.5 μmol m^{-2} s^{-1}. The variations of coefficient values are presented as follows: (*A*) β_c and (*B*) γ_c.

As per Eq. 1 of the FvCB model, Eq. 4 specifies the rate of carboxylation (V_c) as the initial term, and the actual photorespiration rate, indicated as R_p, as the subsequent term. Consequently, R_p can be articulated as follows:

$$R_p = \alpha_c \frac{1-\beta_c C_i}{1+\gamma_c C_i} \Gamma_* \tag{5}$$

In Eq. 5, R_p nonlinearly diminishes as C_i increases. This inverse relationship allows Eq. 5 to be effectively utilized for exploring the dynamic between R_p and C_i across a spectrum of environmental conditions. Moreover, Eq. 5 demonstrates that the values of Γ_* exert a direct influence on R_p. Notably, as C_i approaches 0 μmol mol^{-1}, the R_p at zero intercellular or ambient CO_2 concentration, denoted as R_{p0}, is calculated as $R_{p0} = \alpha_c \Gamma_*$.

The first derivative of Eq. 3 is expressed as follows:

$$\frac{dP_N}{dC_i} = \alpha_c \frac{1-2\beta_c C_i - \beta_c \gamma_c C_i^2 + (\beta_c+\gamma_c)\Gamma_*}{(1+\gamma_c C_i)^2} \tag{6}$$

where dP_N/dC_i is the slope of the P_N–C_i curve, and dP_N/dC_i decreases with increasing C_i. As C_i tends to zero in Eq. 6, dP_N/dC_i equals α_c [1 + (β_c + γ_c)Γ_*], and it is referred to as the initial slope of the P_N–C_i curve (*i.e.*, $\alpha_0 = \alpha_c$ [1 + (β_c + γ_c)Γ]). dP_N/dC_i equals zero when C_i equals to C_i transit points from RuBP-limited to TPU-limited photosynthesis ($C_{i,TPU}$), then dP_N/dC_i will be negative when C_i surpasses $C_{i,TPU}$.

Fig. 2 depicts the relationship between the rate of change of net photosynthesis to intercellular CO_2 concentration (dP_N/dC_i) and C_i itself. It is observed that dP_N/dC_i exhibits a nonlinear decrease as C_i increases. The figure shows that when the value of γ_c is held constant, an increase in the value of β_c leads to a more pronounced curvature in the curve and a steeper rate of decline in dP_N/dC_i with increasing C_i (Fig. 2*A*). In contrast, when the value of β_c is kept constant, a higher value of γ_c results in a less curved profile and a more gradual rate of decrease in dP_N/dC_i as C_i levels rise in high CO_2 concentrations (Fig. 2*B*). These observations highlight the significant impact of the coefficients β_c and γ_c on the dP_N/dC_i–C_i curve, which is crucial for understanding the dynamics of photosynthetic responses to changes in CO_2 concentration. Additionally, Fig. 2 illustrates that the rate of change of P_N with respect to C_i, denoted as dP_N/dC_i, exhibits a gradual decline as the C_i variable is altered.

Therefore, while the dP_N/dC_i = 0, $C_{i,TPU}$ is calculated by:

$$C_{i,TPU} = \frac{\sqrt{(\beta_c+\gamma_c)(1+\gamma_c\Gamma)/\beta_c} - 1}{\gamma_c} \tag{7}$$

And the P_{Nmax} can be obtained as:

$$P_{Nmax} = \alpha_c \left[\frac{\sqrt{\beta_c+\gamma_c} - \sqrt{\beta_c(1+\gamma_c\Gamma_*)}}{\gamma_c} \right]^2 - R_{day} \tag{8}$$

In addition to $C_{i,TPU}$ and P_{Nmax} can be derived from Eqs. 7 and 8, respectively. Likewise, once R_{day} is ascertained, Γ_* can be determined by applying Eq. 3.

A new model for describing the CO_2-response curve of photosynthesis without an explicit R_{day}: Given the enduring challenge in precisely measuring R_{day} in plants – as noted by various studies (Atkin *et al*. 2000, Yin *et al*. 2011, Tcherkez *et al*. 2017); for an exhaustive review, *see* Tcherkez (Tcherkez *et al*. 2017) – we introduce an innovative model crafted to accurately delineate the P_N–C_i curve while mitigating the potential discrepancies in the fitting process that can stem from varying assumptions about R_{day}. This model, henceforth referred to as Model II, is expressed as following equation:

$$P_N = \alpha_{c1}\frac{1-\beta_{c1}C_i}{1+\gamma_{c1}C_i}(C_i-\Gamma) \tag{9}$$

where α_{c1}, β_{c1}, and γ_{c1} are three coefficients that depend on plant characteristics and environmental conditions; Γ is the photorespiratory CO_2-compensation point in the presence of R_{day} (Farquhar *et al*. 1980, Long and Bernacchi 2003). Furthermore, considering the influence of R_{day}, it is anticipated that the coefficients of α_{c1}, β_{c1}, and γ_{c1} in Eq. 9 will differ from those of α_c, β_c, and γ_c in Eq. 3. Similarly, β_{c1} is often designated as the oxygenation term, while γ_{c1} is acknowledged as the saturation term.

In addition, Eq. 9 can be rearranged as:

$$P_N = \alpha_{c1}\frac{1-\beta_{c1}C_i}{1+\gamma_{c1}C_i}C_i - \alpha_{c1}\frac{1-\beta_{c1}C_i}{1+\gamma_{c1}C_i}\Gamma \tag{10}$$

In Eq. 10 the first item is the gross photosynthetic rate, and the second item is the apparent photorespiration rate (R_{pa}) including R_{day}. Therefore, R_{pa} can be expressed as:

$$R_{pa} = \alpha_{c1}\frac{1-\beta_{c1}C_i}{1+\gamma_{c1}C_i}\Gamma \tag{11}$$

In Eq. 11, R_{pa} nonlinearly decreases as C_i increases. Therefore, it can be utilized to explore the relationship between R_{pa} and C_i for all plant species under any environmental conditions. Moreover, Eq. 11 demonstrates that the values of Γ exert a direct influence on R_{pa}. Notably, as C_i approaches 0 μmol mol^{-1}, the R_{pa} at zero intercellular or ambient CO_2 concentration, denoted as R_{pa0}, is calculated as $R_{pa0} = \alpha_{c1}\Gamma$.

The first derivative of Eq. 9 may be expressed as follows:

$$\frac{dP_N}{dC_i} = \alpha_{c1}\frac{1-2\beta_{c1}C_i-\beta_c\gamma_{c1}C_i^2+(\beta_{c1}+\gamma_{c1})\Gamma}{(1+\gamma_{c1}C_i)^2} \tag{12}$$

where dP_N/dC is the slope of the P_N–C curve, and dP_N/dC decreases with increasing C_i. As C_i tends to zero in Eq. 12, dP_N/dC equals to α_{c1} [1 + (β_{c1} + γ_{c1})Γ], and it is referred to as the initial slope of the P_N–C_i curve (*i.e.*, α_0 = α_{c1} [1 + (β_{c1} + γ_{c1})Γ]). dP_N/dC equals zero when C_i equals to $C_{i,TPU}$, then dP_N/dC_i will be negative when C_i surpasses $C_{i,TPU}$.

Therefore, while the dP_N/dC_i = 0, $C_{i,TPU}$ is calculated by:

$$C_{i,TPU} = \frac{\sqrt{(\beta_{c1}+\gamma_{c1})(1+\gamma_{c1}\Gamma)/\beta_{c1}}-1}{\gamma_{c1}} \tag{13}$$

And P_{Nmax} can be obtained as:

$$P_{Nmax} = \alpha_{c1}\left[\frac{\sqrt{\beta_{c1}+\gamma_{c1}}-\sqrt{\beta_{c1}(1+\gamma_{c1}\Gamma)}}{\gamma_{c1}}\right]^2 \tag{14}$$

In addition, $C_{i,TPU}$ and P_{Nmax} can be derived from Eqs. 13 and 14, respectively. Likewise, Γ can be inferred from Eq. 9. It is crucial to recognize that Eqs. 3 and 9 are essentially equivalent in their utility for determining key photosynthetic parameters such as $C_{i,TPU}$ and P_{Nmax} when fitting the P_N–C_i curves. This equivalence underscores the robustness of these equations in capturing the essential characteristics of photosynthetic responses to CO_2 concentrations.

Gas exchange and chlorophyll fluorescence measurement: The P_N–I curves for each study plant were determined using an open-path gas exchange system (*LI-6400*, *Li-Cor*, Lincoln, NE, USA), which was complemented by a leaf chamber fluorometer (*LI-6400-40*, *Li-Cor*). The measurements were conducted between 9:30 and 11:30 h, and from 14:30 to 17:00 h on days with abundant sunlight. An open gas path was utilized for these measurements, with the flow rate adjusted to 500 μmol s^{-1}. The ambient CO_2 concentration was set at 430 μmol mol^{-1} for 13 light intensities, sequentially arranged as follows: 2,000; 1,800; 1,600; 1,400; 1,200; 1,000; 800, 600, 400, 200, 100, 50, 0 μmol(photon) m^{-2} s^{-1} for *I. batatas*, *P. erosus*, *C. annuum*, and *A. esculentus*. The relative humidity of the air was meticulously controlled within the range of 45 to 75%. The plants were given approximately 2 to 3 min to acclimate to the varying light intensities before the measurements were recorded; the completion of an entire P_N–I curve took about 50 min. Post data collection, we employed a mechanistic model of P_N–I within photosynthetic model simulation software (*PMSS*), available in both Chinese and English versions (http://www.zipiao.tech) (*Zipiao Software Development Co., Ltd.*, China), to simulate the P_N–I curves. This analysis determined the saturating irradiance (I_{sat}) to be approximately 1,500 μmol(photon) m^{-2} s^{-1} for *I. batatas* and *P. erosus*, and 2,000 μmol(photon) m^{-2} s^{-1} for *C. annuum* and *A. esculentus*, respectively. Subsequently, P_N–C_i and J–C_i curves were simultaneously recorded at saturating irradiance for 12 CO_2 concentrations, sequentially ordered as follows: 1,400; 1,200; 1,000; 800, 600, 500, 430, 300, 200, 100, 60, and 0 μmol mol^{-1} for *I. batatas*, *P. erosus*, *C. annuum*, and *A. esculentus*. To ensure steady-state conditions, plants were allotted about 5 min to acclimate to the ambient CO_2 in the gas-exchange chamber before the commencement of each P_N–C_i curve, after which the measurements were logged. An automated measurement protocol was implemented to gather photosynthesis-related data, with a minimum waiting time of 3 min and a maximum of 5 min recorded per program cycle. The completion of a single P_N–C_i and J–C_i curve took approximately 50 min.

We employed Eqs. 3 and 9 to discern a suite of pivotal quantitative traits, such as α_c (α_{c1}), P_{Nmax}, Γ_*, Γ,

$C_{i,TPU}$, and R_{day}, as well as the CO_2-response of R_{pa} and R_p from the P_N–C_i curve, respectively. This analytical endeavor was facilitated by the *PMSS*. Additionally, while P_N reached 0 µmol m^{-2} s^{-1}, values for Γ were precisely determined using an interpolation technique, which we deemed as the observed data for the quartet of species under investigation. Furthermore, during the analysis of the P_N–C_i curve, considering that C_a is seldom zero, we designate the P_N corresponding to the minimal C_a value as the observed R_{pa0}. Concurrently, at this minimal C_a value, the P_N values derived from Eq. 9 are treated as the fitted R_{pa0} values. In addition, in this research, we adopted the approach of considering R_{day} as half of dark respiratory rate (R_{dark}), following the methodology introduced by Fila *et al*. (2006).

Statistical analysis: All data are reported as means accompanied by the standard error (mean ± SE, n = 3). Statistical analysis was conducted using one-way analysis of variance (*ANOVA*). To assess the significance of differences between the model-estimated values and the actual observations, a paired-sample t-test was applied at the 5% significance level (p<0.05). All statistical procedures were carried out with the *SPSS 18.5* software package (*SPSS*, Chicago, Illinois, USA). Figures were generated using *Origin 2021* and further refined with *Adobe Illustrator CS5*. The goodness-of-fit between the model estimated values and observed data was evaluated using the coefficient of determination (R^2), computed as R^2 = 1 – SSE/SST, where SSE represents the sum of squared errors and SST denotes the total sum of squares.

Results

CO_2-response curves of photosynthesis for four C_3 species: The CO_2-response curve of net CO_2 uptake (P_N–C_a) exhibited the generally expected trend, as shown in Fig. 3. The photosynthetic activity in the four plant species was primarily limited by the kinetics of Rubisco activity and RuBP carboxylation.

Additionally, our findings indicate that for *P. erosus* at high CO_2 concentrations exceeding about 900 µmol mol^{-1}, the net CO_2 uptake (P_N) decreases (Fig. 3*B*). The C_a at which P_N was the maximum (P_{Nmax}) is described by $C_{a,TPU}$ and was lowest for *P. erosus* and highest for *C. annuum* (*ca*. 1,330 µmol mol^{-1}) with intermediate values for *I. batatas* and *A. esculentus* (Fig. 3); it should be noted that P_N for *C. annuum* did not reach saturation within the values of C_a applied for the P_N–C_a curve and hence values for $C_{a,TPU}$ (and P_{Nmax}) are an extrapolation (Fig. 3*C*). Furthermore, our results demonstrate no significant difference between the values obtained using Eq. 3 or Eq. 9 and the observed data for key photosynthetic parameters, such as P_{Nmax}, Γ, and $C_{a,TPU}$, as derived from the CO_2-response curves of the four C_3 plant species (Table 1). The strong fit provided by Eqs. 3 and 9 across the CO_2-response curves confirm its effectiveness as a mathematical framework for studying plant photosynthetic processes.

Table 1 demonstrates that certain pivotal parameters, such as P_{Nmax} and $C_{a,TPU}$, calculated using either Eq. 3 or Eq. 9, closely approximate the observed values. Additionally, the values of Γ calculated using Eq. 9 are in close agreement with the observed data, with the exception of *A. esculentus*. Furthermore, the values of R_{pa0} calculated

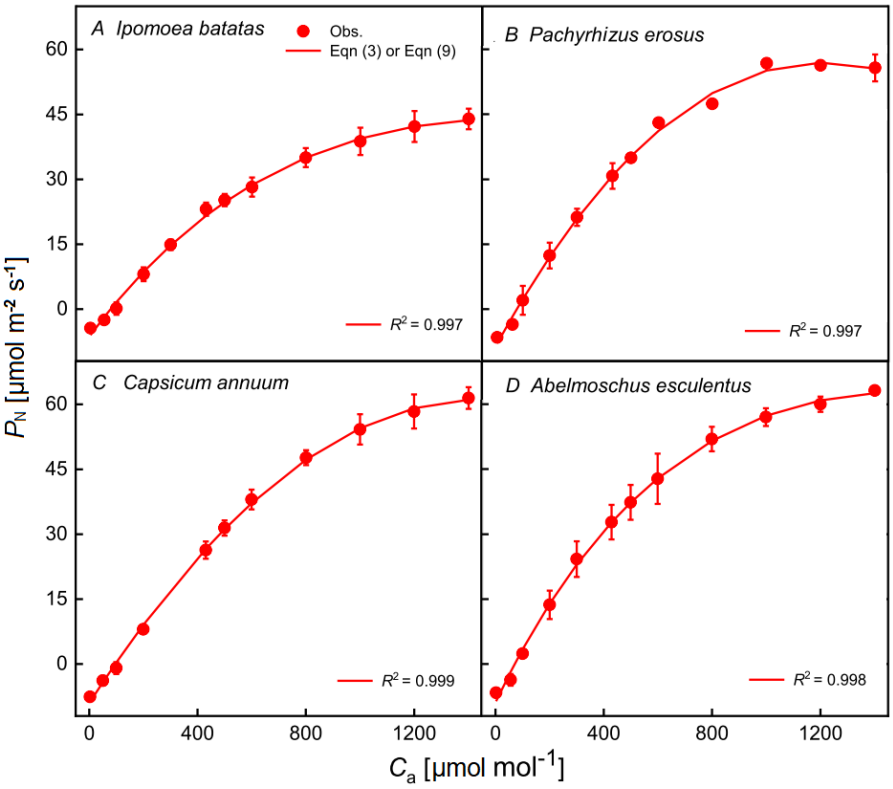

Fig. 3. CO_2-response curves of photosynthesis (P_N) for four C_3 species. The species are as follows: (*A*) *Ipomoea batatas*, (*B*) *Pachyrhizus erosus*, (*C*) *Capsicum annuum*, and (*D*) *Abelmoschus esculentus*. *The red dots* on the curves correspond to the points calculated by Eq. 3 or Eq. 9. Each data point represents the mean values ± standard error (SE), with a sample size of n = 3 for each measurement.

Table 1. Observed data and results estimated by Eq. 3 or Eq. 9 for four C_3 species (mean ± SE, n = 3). Estimated and observed parameter values within one plant which are statistically significantly different (p<0.05) are annotated with *different superscript letter*.

	Ipomoea batatas		*Pachyrhizus erosus*		*Capsicum annuum*		*Abelmoschus esculentus*	
	Eq. 3	Obs.	Eq. 3	Obs.	Eq. 3	Obs.	Eq. 3	Obs.
α_0 [μmol m^{-2} s^{-1}]	0.079 ± 0.006	-	0.113 ± 0.004	-	0.098 ± 0.003	-	0.129 ± 0.016	-
$C_{a,TPU}$ [μmol mol^{-1}]	1,426.67 ± 78.60^a	1,399.82 ± 0.28^a	1,216.67 ± 38.44^a	1,134.09 ± 133.48^a	1,466.67 ± 46.67^a	1,400.01 ± 0.40^a	1,470.05 ± 96.44^a	1,400.43 ± 0.37^a
P_{Nmax} [μmol m^{-2} s^{-1}]	43.49 ± 1.94^a	43.96 ± 1.38^a	57.19 ± 0.93^a	57.34 ± 1.01^a	61.38 ± 1.83^a	61.47 ± 1.44^a	62.90 ± 0.46^a	63.21 ± 0.40^a
Γ_* [μmol mol^{-1}]	54.68 ± 5.31	-	56.94 ± 7.24	-	70.65 ± 1.66	-	46.52 ± 1.87	-
R_{day} [μmol m^{-2} s^{-1}]	1.78 ± 0.06	-	2.17 ± 0.17^a	-	2.33 ± 0.17	-	2.62 ± 0.27	-
R_{p0} [μmol m^{-2} s^{-1}]	4.46 ± 0.27^a	-	6.38 ± 0.94^a	-	6.75 ± 0.25^a	-	5.86 ± 0.93^a	-
R^2	0.997	-	0.997	-	0.999	-	0.998	-
	Eq. 9	Obs.	Eq. 9	Obs.	Eq. 9	Obs.	Eq. 9	Obs.
α_0 [μmol m^{-2} s^{-1}]	0.079 ± 0.006	-	0.113 ± 0.004	-	0.098 ± 0.003	-	0.129 ± 0.016	-
$C_{a,TPU}$ [μmol mol^{-1}]	1,426.67 ± 78.60^a	1,399.82 ± 0.28^a	1,216.67 ± 38.44^a	1,134.09 ± 133.48^a	1,466.67 ± 46.67^a	1,400.01 ± 0.40^a	1,470.05 ± 96.44^a	1,400.43 ± 0.37^a
P_{Nmax} [μmol m^{-2} s^{-1}]	43.49 ± 1.94^a	43.96 ± 1.38^a	57.19 ± 0.93^a	57.34 ± 1.01^a	61.38 ± 1.83^a	61.47 ± 1.44^a	62.90 ± 0.46^a	63.21 ± 0.40^a
Γ [μmol mol^{-1}]	76.91 ± 7.17^a	96.25 ± 11.45^a	77.08 ± 7.53^a	91.90 ± 9.72^a	96.06 ± 1.62^a	109.10 ± 7.51^a	69.47 ± 2.^{3}3b	83.01 ± 2.^{0}9a
R_{pa0} [μmol m^{-2} s^{-1}]	6.06 ± 0.44^a	4.38 ± 0.04^b	7.90 ± 1.02^a	6.50 ± 0.50^a	8.79 ± 0.10^a	7.56 ± 0.30^b	8.61 ± 1.09^a	6.64 ± 0.59^a
R^2	0.997	-	0.997	-	0.999	-	0.998	-

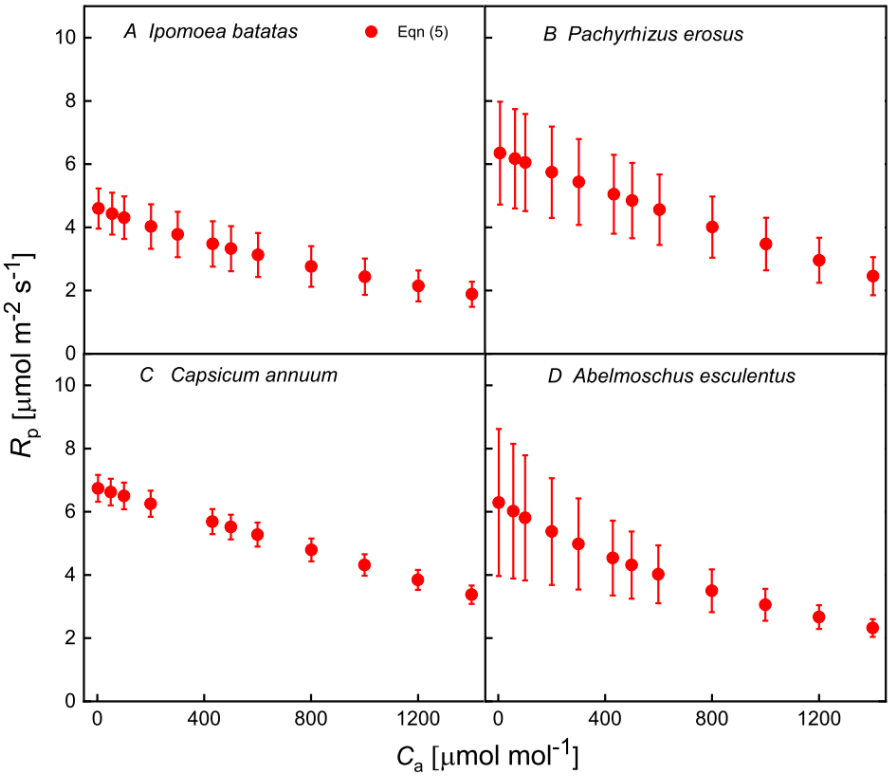

Fig. 4. CO_2-response curves of photorespiratory rate (R_p) for four C_3 species. The species are as follows: (*A*) *Ipomoea batatas*, (*B*) *Pachyrhizus erosus*, (*C*) *Capsicum annuum*, and (*D*) *Abelmoschus esculentus*. *The solid red dots* on the graph denote the values calculated by Eq. 5. Each data point represents the mean values ± standard error (SE), with a sample size of n = 3 for each measurement.

using Eq. 9 align well with the observed values, except for *I. batatas* and *C. annuum*.

CO_2-response curves of R_p and R_{pa} for four C_3 species under saturating irradiance: Figs. 4 and 5 elegantly demonstrate that both the actual photorespiratory rate (R_p) and the apparent photorespiratory rate (R_{pa}) exhibit a nonlinear decline with an increase in ambient CO_2 concentration (C_a). This observation suggests that R_p and R_{pa} share analogous sensitivities to changes in CO_2 concentrations.

Discussion

P_N–C_i curves: The FvCB model, first introduced by Farquhar, von Caemmerer, and Berry in 1980, has become an indispensable tool for deciphering and quantifying the kinetics of carbon fixation and the intricate relationship between P_N and C_i (Bernacchi *et al.* 2013, Flexas *et al.* 2016, Norby *et al.* 2017, Rogers *et al.* 2017, Silva-Pérez *et al.* 2017, Ye *et al.* 2025a). Celebrated for its mechanistic rigor, the FvCB model plays a pivotal role in assessing photosynthetic acclimation and predicting the extensive

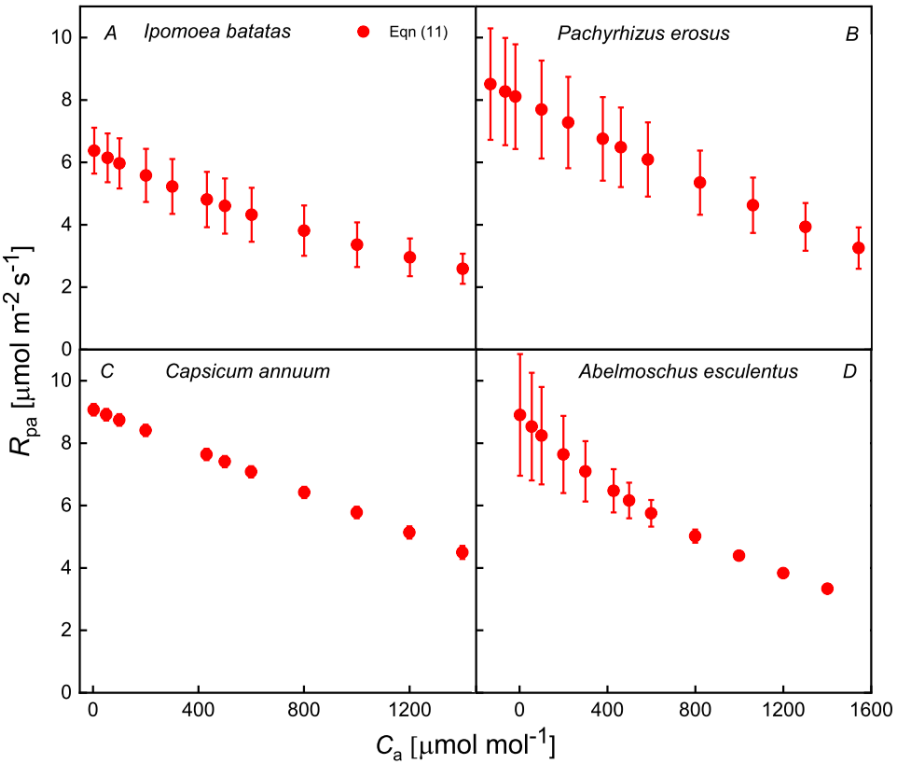

Fig. 5. CO_2-response curves of apparent photorespiratory rate (R_{pa}) for four C_3 species. The species are as follows: (*A*) *Ipomoea batatas*, (*B*) *Pachyrhizus erosus*, (*C*) *Capsicum annuum*, and (*D*) *Abelmoschus esculentus*. *The solid red dots* on the graph denote the values calculated by Eq. 11. Each data point represents the mean values ± standard error (SE), with a sample size of n = 3 for each measurement.

impacts of climate change on terrestrial and global ecosystems, a consensus supported by an abundance of scholarly research (Dubois *et al*. 2007, Busch and Sage 2017, Walker *et al*. 2017, Smith *et al*. 2019, Han *et al.* 2020, Yin *et al*. 2021, 2024).

In our study, a meticulous analysis confirmed that the P_N–C_a relationship adhered to the anticipated patterns, revealing inherent physiological constraints on photosynthesis across four distinct C_3 plant species. In a normal environment, photosynthesis was primarily limited by the carboxylation efficiency of the Rubisco enzyme and the availability of RuBP, key components of the Calvin cycle, as illustrated in Fig. 3.

Our study validated the efficacy of two mathematical models, Eqs. 3 and 9, which were employed to calculate key photosynthetic parameters. The calculated values were closely aligned with observed data, reflecting the high accuracy and reliability of these models. This was evident in the comparison of parameters such as P_{Nmax}, Γ, and $C_{a,TPU}$, derived from the P_N–C_a curves of the four C_3 plant species (Table 1). Our results indicated no significant differences between the key photosynthetic parameters derived from Eqs. 3 and 9 and the corresponding observed values, except for R_{pa0}. Furthermore, the fitting curves highly matched the observed data points, showing high R^2 values (Table 1). Therefore, Eqs. 3 and 9 are two robust models, and we can utilize the derived models from these to investigate the response patterns of R_p and R_{pa} to C_a. However, it should be noted that the values of Γ calculated using Eq. 9 are in close agreement with the observed data, except for *A. esculentus* (Table 1). The discrepancy is attributed to the relatively large CO_2 gradient intervals (50 and 100 μmol mol^{-1}) employed in our study. As a result, the Γ values estimated by the interpolation method are likely to be lower than the observed values (Table 1). To achieve a more accurate estimation of the Γ values for these plants, we recommend incorporating additional CO_2 concentration gradients, such as 70 μmol mol^{-1}, at low CO_2 concentrations. Furthermore, the values of R_{pa0} calculated using Eq. 9 align well with the observed values, except for *I. batatas* and *C. annuum* (Table 1). The issue arises because the CO_2 gradient intervals used in our study (50 and 100 μmol mol^{-1}) are too large. As a result, the R_{pa0} values estimated by Eq. 9 are likely to be higher than the observed values for *I. batatas* and *C. annuum*. To obtain a more accurate estimate of the R_{pa0} values for these plants, we recommend incorporating additional CO_2 concentration gradients, such as 5, 10, 20, and 40 μmol mol^{-1}, particularly at low CO_2 concentrations.

In addition, it is important to note that the curvature of the P_N–C_i curves and the derived parameters (P_{Nmax}, Γ, and $C_{a,TPU}$) are influenced not only by biochemical factors but also by leaf anatomy and g_m (Flexas *et al.* 2016, Yin *et al.* 2021). The g_m significantly affects the slope of the P_N–C_i relationship, particularly in the Rubisco-limited region (Long and Bernacchi 2003, Ye *et al.* 2024a, 2025b). In our model, the coefficients in our models (α_c, β_c, and γ_c) in Model I and their counterparts in Model II are, by design, composite parameters (Ye *et al.* 2025b). They inherently encapsulate the combined effects of both biochemical (*e.g.*, V_{cmax}, $C_{a,TPU}$) and diffusional limitations, including the significant influence of g_m on the transition between these limitations and the overall shape of the curve (Ye *et al.* 2024a, 2025b). In our model, although the influence of g_m is implicitly integrated into the empirical coefficients (such as α_c, β_c, and γ_c), which allows us to

accurately fit the P_N–C_i curves and estimate parameters from standard gas-exchange data, future work could explore explicitly incorporating g_m into the model's structure. This would further enhance its mechanistic foundation and enable a more precise distinction between biochemical and diffusional limitations.

Characterizing R_p–C_i and R_{pa}–C_i curves using new models: To the best of our knowledge, no current model has quantitatively explored the CO_2-responsiveness of R_p and R_{pa}. However, our study provides evidence that the quantitative relationship between R_p and R_{pa}, which exhibits a nonlinear increase with CO_2, can be described by Eqs. 5 and 11. This relationship has been validated across the four C_3 plant species included in this study, as depicted in Fig. 4. These figures visually capture the nonlinear relationship between R_p and R_{pa} with increasing C_a, suggesting a similar sensitivity to CO_2 fluctuations for both parameters. This similarity suggests a shared regulatory mechanism in response to fluctuating CO_2 concentrations, as previously discussed by Farquhar and Busch (2017) and Yin and Struik (2012).

By employing Eqs. 5 and 11, researchers can pinpoint the specific junctures where photorespiration constrains the photosynthetic capacity of plants under diverse environmental conditions. This understanding is crucial for elucidating the intricate interplay between plant physiology and environmental factors, as well as their collective impact on plant growth and productivity (Drake *et al*. 1997, Leakey *et al*. 2006, Yin and Struik 2012, Siqueira *et al*. 2025). Furthermore, Eqs. 5 and 11 enable the comparison of photorespiratory responses across various plant species, assisting in the identification of species-specific adaptations to environmental stressors. These equations are also indispensable for comprehensively characterizing CO_2-response curves for both R_{pa} and R_p across various plants. They provide a mathematical framework to analyze how environmental conditions, such as light intensity, temperature, and atmospheric CO_2 and O_2 concentrations, influence photorespiration. Fundamentally, Eqs. 5 and 11 are sophisticated analytical instruments, not just mathematical constructs. They can reveal the intricate interplay between plants and their environment. These equations enhance our comprehension of how plants may adapt to future atmospheric conditions under global change. This understanding is pivotal in guiding the development of plant varieties better suited to thrive in elevated CO_2 environments, with profound implications for both agricultural practices and ecosystem management.

It is crucial to emphasize that the accurate portrayal of the CO_2-response curve for R_p, as delineated by Eq. 5, hinges on the precise assignment of values to R_{day}. Therefore, the exact measurement or ascertainment of R_{day} is vital for a rigorous quantitative study of R_p in C_3 plants. On the other hand, Eq. 11 offers a distinct advantage by enabling the quantitative analysis of the CO_2-response curve for R_{pa} without necessitating the consideration of specific R_{day} values for C_3 plants. As a result, Eq. 11 stands out as an indispensable tool for exploring the photoprotective effects of R_{pa} across a diverse array of environmental conditions in C_3 plants. Moreover, the accuracy of our model's predictions is fundamentally linked to the caliber of the input data. The clear correlation between the precision of the model fit and the quality of the measured data underscores the critical importance of thorough data collection and meticulous analysis. It is through this rigorous process that we can ensure the robustness and reliability of our model's projections. Essentially, the model serves as a mirror to the data it processes, reflecting the intricacies and subtleties of the biological phenomena it aims to capture. This realization highlights the imperative for ongoing efforts to enhance data quality, thereby bolstering the predictive power of our model. Consequently, to accurately simulate and depict the P_N–C_a curves under low CO_2 concentrations, we advocate for the inclusion of specific data points. For C_3 species, we propose the addition of points at 20, 40, 60, and 80 μmol mol^{-1}. These increments will furnish a comprehensive dataset, which is vital for achieving a detailed and precise representation of the curves.

Conclusion: In conclusion, this study successfully developed and validated two innovative models – Model I and Model II – that effectively characterize the CO_2-response curves of photosynthesis and photorespiration in C_3 plants. These models address the limitations of the Farquhar–von Caemmerer–Berry (FvCB) model by directly estimating critical photosynthetic parameters such as P_{Nmax}, Γ, R_{pa0}, and $C_{a,TPU}$. Our results demonstrate that both models provide accurate and reliable predictions of photosynthetic and photorespiratory responses under varying CO_2 concentrations, with strong alignment between model-derived parameters and observed data.

The validation of these models across four C_3 plant species (*Ipomoea batatas*, *Pachyrhizus erosus*, *Capsicum annuum*, and *Abelmoschus esculentus*) highlights their potential for broader application in plant physiological research. The models' ability to accurately depict the dynamic behavior of photosynthesis and photorespiration under various environmental conditions makes them valuable tools for understanding plant responses to atmospheric CO_2 fluctuations. This is particularly relevant in the context of climate change, where elevated CO_2 concentrations and altered environmental conditions are expected to impact plant growth, productivity, and ecosystem functioning.

Our study emphasizes the importance of high-quality data for accurate model predictions. The precision of the model fits is directly linked to the quality of input data, underscoring the need for meticulous data collection and analysis. To further enhance the robustness of these models, we recommend incorporating additional CO_2 concentration gradients, especially at low CO_2 concentrations, to improve the accuracy of estimated parameters such as Γ and R_{pa0}. Future research should also explore the application of these models to a wider range of plant species and environmental conditions, including C_4 plants, to assess their universal applicability.

Overall, the development of Model I and Model II represents a significant advancement in the field of plant photosynthesis modeling. By providing a more direct and accessible method to estimate critical parameters, such as P_{Nmax}, Γ, R_{pa0}, and $C_{a,TPU}$, these models can streamline photosynthetic phenotyping, aiding in the rapid screening of crop varieties for enhanced photosynthetic efficiency and resilience to environmental stress. Furthermore, these models provide a comprehensive framework for studying the complex interactions between plant physiology and environmental factors, offering valuable insights for agricultural practices, ecosystem management, and climate change adaptation strategies. This is particularly crucial for future-proofing agriculture against climate change, as these models offer a refined tool to predict how rising CO_2 levels and fluctuating environments will impact carbon assimilation and photorespiratory losses in C_3 plants, which form the basis of global food supply. Future work should focus on refining the CO_2 concentration gradients used in experiments to enhance the accuracy of key parameters such as Γ and R_{pa0}. Additionally, expanding the application of the models to a broader range of plant species and environmental conditions, including C_4, CAM plants, and varying light and temperature regimes, is essential. Further validation under real-world field conditions and integration with climate change scenarios will also be crucial to fully realize the models' potential for predicting plant responses to future environments. Importantly, we need to explore the relationships between the coefficients (such as α_c, β_c, and γ_c) and the key components of photosynthesis, including the Rubisco enzyme, RuBP regeneration, and triose phosphate utilization rates. This will enhance our understanding of the underlying mechanisms driving photosynthetic responses.

References

Atkin O.K., Evans J.R., Ball M.C. *et al.*: Leaf respiration of snow gum in the light and dark. Interactions between temperature and irradiance. – Plant Physiol. **122**: 915-924, 2000.

Baker N.R.: Chlorophyll fluorescence: a probe of photosynthesis *in vivo*. – Annu. Rev. Plant Biol. **59**: 89-113, 2008.

Barbour M.M., Evans J.R., Simonin K.A., von Caemmerer S.: Online CO_2 and H_2O oxygen isotope fractionation allows estimation of mesophyll conductance in C_4 plants, and reveals that mesophyll conductance decreases as leaves age in both C_4 and C_3 plants. – New Phytol. **210**: 875-889, 2016.

Bernacchi C.J., Bagley J.E., Serbin S.P. *et al.*: Modelling C_3 photosynthesis from the chloroplast to the ecosystem. – Plant Cell Environ. **36**: 1641-1657, 2013.

Busch F.A., Sage R.F.: The sensitivity of photosynthesis to O_2 and CO_2 concentration identifies strong Rubisco control above the thermal optimum. – New Phytol. **213**: 1036-1051, 2017.

Chang Y., Latham J., Licht M., Wang L.: A data-driven crop model for maize yield prediction. Commun. Biol. **6**: 439, 2023.

Drake B.G., Gonzàlez-Meler M.A., Long S.P.: More efficient plants: a consequence of rising atmospheric CO_2? – Annu. Rev. Plant Biol. **48**: 609-639, 1997.

Dubois J.-J.B., Fiscus E.L., Booker F.L. *et al.*: Optimizing the statistical estimation of the parameters of the Farquhar–von Caemmerer–Berry model of photosynthesis. – New Phytol. **176**: 402-414, 2007.

Farazdaghi H., Edwards G.E.: A model for photosynthesis and photorespiration in C_3 plants based on the biochemistry and stoichiometry of the pathways. – Plant Cell Environ. **11**: 799-809, 1988.

Farquhar G.D., Busch F.A.: Changes in the chloroplastic CO_2 concentration explain much of the observed Kok effect: a model. – New Phytol. **214**: 570-584, 2017.

Farquhar G.D., von Caemmerer S., Berry J.A.: A biochemical model of photosynthetic CO_2 assimilation in leaves of C_3 species. – Planta **149**: 78-90, 1980.

Fila G., Badeck F.-W., Meyer S. *et al.*: Relationships between leaf conductance to CO_2 diffusion and photosynthesis in micropropagated grapevine plants, before and after *ex vitro* acclimatization. – J. Exp. Bot. **57**: 2687-2695, 2006.

Flexas J., Díaz-Espejo A., Conesa M.A. *et al.*: Mesophyll conductance to CO_2 and Rubisco as targets for improving intrinsic water use efficiency in C_3 plants. – Plant Cell Environ. **39**: 965-982, 2016.

Gregory L.M., McClain A.M., Kramer D.M. *et al.*: The triose phosphate utilization limitation of photosynthetic rate: out of global models but important for leaf models. – Plant Cell Environ. **44**: 3223-3226, 2021.

Han T., Zhu G., Ma J. *et al.*: Sensitivity analysis and estimation using a hierarchical Bayesian method for the parameters of the FvCB biochemical photosynthetic model. – Photosynth. Res. **143**: 45-66, 2020.

Harley P.C., Sharkey T.D.: An improved model of C_3 photosynthesis at high CO_2: reversed O_2 sensitivity explained by lack of glycerate reentry into the chloroplast. – Photosynth. Res. **27**: 169-178, 1991.

Hu H., Jiang W., Fan X.: Estimating CO_2 response in a mixed broadleaf forest using the dynamic assimilation technique. – BMC Plant Biol. **25**: 79, 2025.

Joshi J., Stocker B.D., Hofhansl F. *et al.*: Towards a unified theory of plant photosynthesis and hydraulics. – Nat. Plants **8**: 1304-1316, 2022.

Joubert D., Zhang N., Berman S.R. *et al.*: A small dynamic leaf-level model predicting photosynthesis in greenhouse tomatoes. – PLoS ONE **18**: e0275047, 2023.

Kieffer C., Kaur N., Li J. *et al.*: Photosynthetic responses of switchgrass to light and CO_2 under different precipitation treatments. – Glob. Change Biol.-Bioenergy **16**: e13138, 2024.

Kromdijk J., Głowacka K., Long S.P.: Predicting light-induced stomatal movements based on the redox state of plastoquinone: theory and validation. – Photosynth. Res. **141**: 83-97, 2019.

Lawson T., Oxborough K., Morison J.I.L., Baker N.R.: Responses of photosynthetic electron transport in stomatal guard cells and mesophyll cells in intact leaves to light, CO_2, and humidity. – Plant Physiol. **128**: 52-62, 2002.

Leakey A.D.B., Uribelarrea M., Ainsworth E.A. *et al.*: Photosynthesis, productivity, and yield of maize are not affected by open-air elevation of CO_2 concentration in the absence of drought. – Plant Physiol. **140**: 779-790, 2006.

Li Y.L., Liu X.G., Hao K. *et al.*: Light-response curve of photosynthesis and model fitting in leaves of *Mangifera indica* under different soil water conditions. – Photosynthetica **57**: 796-803, 2019.

Liu J., Ryu Y., Luo X. *et al.*: Evidence for widespread thermal acclimation of canopy photosynthesis. – Nat. Plants **10**: 1919-1927, 2024.

Long S.P., Bernacchi C.J.: Gas exchange measurements, what can they tell us about the underlying limitations to photosynthesis? Procedures and sources of error. – J. Exp. Bot. **54**: 2393-2401, 2003.

Norby R.J., Gu L., Haworth I.C. *et al.*: Informing models through empirical relationships between foliar phosphorus, nitrogen and photosynthesis across diverse woody species in tropical forests of Panama. – New Phytol. **215**: 1425-1437, 2017.

Peisker M.: Models of carbon metabolism in C_3-C_4 intermediate plants as applied to the evolution of C_4 photosynthesis. – Plant Cell Environ. **9**: 627-635, 1986.

Poirier-Pocovi M., Lothier J., Buck-Sorlin G.: Modelling temporal variation of parameters used in two photosynthesis models: influence of fruit load and girdling on leaf photosynthesis in fruit-bearing branches of apple. – Ann. Bot.-London **121**: 821-832, 2018.

Rizza F., Pagani D., Stanca A.M., Cattivelli L.: Use of chlorophyll fluorescence to evaluate the cold acclimation and freezing tolerance of winter and spring oats. – Plant Breeding **120**: 389-396, 2001.

Rogers A., Serbin S.P., Ely K.S. *et al.*: Terrestrial biosphere models underestimate photosynthetic capacity and CO_2 assimilation in the Arctic. – New Phytol. **216**: 1090-1103, 2017.

Sharkey T.D., Bernacchi C.J., Farquhar G.D., Singsaas E.L.: Fitting photosynthetic carbon dioxide response curves for C_3 leaves. – Plant Cell Environ. **30**: 1035-1040, 2007.

Silva-Pérez V., Furbank R.T., Condon A.G., Evans J.R.: Biochemical model of C_3 photosynthesis applied to wheat at different temperatures. – Plant Cell Environ. **40**: 1552-1564, 2017.

Siqueira J.A., Martins A.O., Wakin T. *et al.*: The modulation of growth and metabolism in *Solanum lycopersicum* contrast with the leaf-specific regulation of wild tomato species. – Plant Cell Environ. **48**: 1201-1214, 2025.

Smith N.G., Keenan T.F., Prentice I.C. *et al.*: Global photosynthetic capacity is optimized to the environment. – Ecol. Lett. **22**: 506-517, 2019.

Sun J., Sun J., Feng Z.: Modelling photosynthesis in flag leaves of winter wheat (*Triticum aestivum*) considering the variation in photosynthesis parameters during development. – Funct. Plant Biol. **42**: 1036-1044, 2015.

Tcherkez G., Gauthier P., Buckley T.N. *et al.*: Leaf day respiration: low CO_2 flux but high significance for metabolism and carbon balance. – New Phytol. **216**: 986-1001, 2017.

Vialet-Chabrand S.R.M., Matthews J.S.A., McAusland L. *et al.*: Temporal dynamics of stomatal behavior: modelling and implications for photosynthesis and water use. – Plant Physiol. **174**: 603-613, 2017.

Walker A.P., Quaife T., van Bodegom P.M. *et al.*: The impact of alternative trait-scaling hypotheses for the maximum photosynthetic carboxylation rate (V_{cmax}) on global gross primary production. – New Phytol. **215**: 1370-1386, 2017.

Wu Q., Zhang T., Li C.R. *et al.*: Photosynthetic CO_2 response to soil water and its simulation using different models in leaves of two species. – Photosynthetica **58**: 790-798, 2020.

Xue W., Luo H., Carriquí M. *et al.*: Quantitative expression of mesophyll conductance temperature response in the FvCB model and impacts on plant gas exchange estimations. – Agr. Forest Meteorol. **325**: 109153, 2022.

Ye Z.P., He J.Q., An T. *et al.*: Influences of residual stomatal conductance on the intrinsic water use efficiency of two C_3 and two C_4 species. – Agr. Water Manage. **306**: 109136, 2024a.

Ye Z.P., Hu W.H., Zhou S.X. *et al.*: Limitations of the Farquhar–von Caemmerer–Berry model in estimating the maximum electron transport rate: evidence from four C_3 species. – Biology **14**: 630, 2025a.

Ye Z.P., Yang X.L., Ye Z.W.Y. *et al.*: Evaluating photosynthetic models and their potency in assessing plant responses to changing oxygen concentrations: a comparative analysis of A_n–C_a and A_n–C_i curves in *Lolium perenne* and *Triticum aestivum*. – Front. Plant Sci. **16**: 1575217, 2025b.

Ye Z.P., Zhou S.X., Yang X.L. *et al.*: Light curve parametrization of three rice (*Oryza sativa* L.) cultivars based on mechanistic models. – Photosynthetica **62**: 305-313, 2024b.

Yin X.Y., Amthor J.S.: Estimating leaf day respiration from conventional gas exchange measurements. – New Phytol. **241**: 52-58, 2024.

Yin X.Y., Busch F.A., Struik P.C., Sharkey T.D.: Evolution of a biochemical model of steady-state photosynthesis. – Plant Cell Environ. **44**: 2811-2837, 2021.

Yin X.Y., Struik P.C.: Mathematical review of the energy transduction stoichiometries of C_4 leaf photosynthesis under limiting light. – Plant Cell Environ. **35**: 1299-1312, 2012.

Yin X.Y., Struik P.C., Romero P. *et al.*: Using combined measurements of gas exchange and chlorophyll fluorescence to estimate parameters of a biochemical C_3 photosynthesis model: a critical appraisal and a new integrated approach applied to leaves in a wheat (*Triticum aestivum*) canopy. – Plant Cell Environ. **32**: 448-464, 2009.

Yin X.Y., Sun Z.P., Struik P.C. *et al.*: Using a biochemical C_4 photosynthesis model and combined gas exchange and chlorophyll fluorescence measurements to estimate bundle-sheath conductance of maize leaves differing in age and nitrogen content. – Plant Cell Environ. **34**: 2183-2199, 2011.

Yin X.Y., van Oijen M., Schapendonk A.H.C.M.: Extension of a biochemical model for the generalized stoichiometry of electron transport limited C_3 photosynthesis. – Plant Cell Environ. **27**: 1211-1222, 2004.

Zheng Y., Zhao Z., Zhou J.J., Zhou H.: Evaluations of different leaf and canopy photosynthesis models: a case study with black locust (*Robinia pseudoacacia*) plantations on a Loess Plateau. – Pak. J. Bot. **44**: 531-539, 2012.